J of Nuclear Medicine Technology, first published online November 10, 2017 as doi:10.2967/jnmt.117.199042

Imaging of the thyroid and parathyroid using a cardiac cadmium zinc telluride camera: Phantom studies

(Cardiac CZT camera for neck imaging)

Yosuke Miyazaki, MSc[1)], Yasuhiro Kato, BSc[1)], Akira Imoto[2)], Kazuki Fukuchi, MD, PhD[1)]

[1)] Division of Medical Technology and Science, Department of Medical Physics and Engineering, Course of Health Science, Osaka University Graduate School of Medicine, Suita, Osaka, Japan

[2)] Department of Radiology, National Cerebral and Cardiovascular Center, Suita, Osaka, Japan

Address correspondence to: Kazuki Fukuchi, MD

Division of Medical Technology and Science, Department of Medical Physics and Engineering, Course of Health Science, Osaka University Graduate School of Medicine, 1-7 Yamadaoka, Suita, Osaka 565-0871, JAPAN.

Tel: +81-6-6879-2563; Fax: +81-6-6879-2563

E-mail: kfukuchi@sahs.med.osaka-u.ac.jp

Abstract

Purpose: Cadmium zinc telluride (CZT) detectors have recently been introduced to the field of clinical nuclear cardiology. However, the feasibility of using them for organs other than the heart remains unclear. The aim of this study was to evaluate the potential of a cardiac CZT camera to acquire thyroid and parathyroid images. We used custom-made phantoms and the currently available standard protocols for CZT, instead of a sodium-iodine scintillation (NaI) camera.

Materials and Methods: Thyroid phantoms with or without parathyroid adenomas were made from agar using radiopharmaceuticals (^{99m}Tc or ^{123}I) and imaged using CZT and NaI cameras. Using the CZT camera data, we prepared maximum intensity projection (MIP) images and planar equivalent (PE) images. Image counts were compared to those from the NaI camera, and the radioactivity of the phantoms was measured. For parathyroid imaging, three different protocols with the NaI camera were tested using MIP images.

Results: For thyroid imaging, MIP could provide images as clear as those obtained from the NaI camera. The radioactivity and image counts correlated better for the PE images than the MIP images, especially for ^{123}I images. We succeeded in obtaining clear parathyroid adenoma images from MIP images using all three protocols.

Conclusions: A cardiac CZT camera can effectively perform qualitative and quantitative assessments of the thyroid and parathyroid organs.

Keywords: cadmium zinc telluride (CZT), Thyroid Imaging, Parathyroid Imaging, dual-isotope acquisition

Introduction

Recently, semiconductor cadmium zinc telluride (CZT) detectors have been introduced to the field of cardiovascular nuclear medicine. These CZT-based cameras have better sensitivity and spatial resolution than a conventional gamma camera composed of sodium-iodine scintillation detectors (NaI camera) (*1-6*). Gambhir et al. report that CZT-single photon emission computed tomography (SPECT) has 10-fold better sensitivity and approximately 2-fold better spatial resolution than a NaI camera (*6*). This marked increase in sensitivity results in a reduction of acquisition time and the radiopharmaceutical dosage (*1-3,5-7*).

In addition, CZT-SPECT has better energy resolution than a NaI camera. Takahashi et al. report that the energy resolution of CZT-SPECT is 5%, whereas the energy resolution of a NaI camera is 10% (*4*). Therefore, CZT-SPECT has the potential to separate the primary photons of ^{99m}Tc and ^{123}I, which are very close, and provides better quality dual-isotope simultaneous imaging (*8,9*).

Although CZT-SPECT has the remarkable above-mentioned advantage for nuclear medicine imaging, it is currently only applied clinically for cardiovascular and breast imaging (*2*). If cardiac CZT-SPECT were to be used for focused imaging of other organs, the same advantages are to be expected. To make this possible, however, there are some problems that need to be overcome. First, the current cardiac CZT-SPECT can acquire only tomographic images and not planar images. Second, the field of view of the apparatus is limited (*2,3*). Even with these limitations, it should be possible to image small and superficial organs using a cardiac CZT-SPECT; therefore, we assumed that the thyroid and parathyroid organs would be suitable for this imaging modality.

The aim of this study was to verify the ability to use cardiac CZT-SPECT for imaging of the thyroid and parathyroid. Thyroid and parathyroid adenoma phantoms were fabricated to use in simulation studies that were performed using current clinical thyroid and parathyroid scintigraphy protocols (*10-18*).

Materials and Methods

Thyroid and parathyroid adenoma phantoms

A thyroid phantom mold was made from potassium alginate and sodium alginate for modeling the normal-sized thyroid glands as a reference (*19-21*). The length, width, and depth of the thyroid phantom were 60, 20, and 15 mm, respectively. Agar solution and radiopharmaceuticals were then poured into the mold and stirred until the concentration of radioactivity was homogeneous. After 30 minutes, the agar solidified and was usable as a thyroid phantom. A parathyroid adenoma phantom was made using a similar method. We determined that it had a diameter of 8 mm and cylindrical height of 7 mm based on the parathyroid adenomas resected from the patients (*22,23*). This phantom was fixed to the lower quadrant of the left lobe of the thyroid phantom using a needle. Thyroid phantoms with or without a parathyroid adenoma phantom were fixed in the center of a 1500-ml cylindrical plastic bottle (30 cm circumference) filled with radiotracer-containing water, which was used to simulate an adult neck with background activity.

Thyroid imaging

We prepared several thyroid phantoms with various concentrations of ^{99m}Tc pertechnetate or ^{123}I-15-(p-Iodophenyl)-3-methylpentadecanoic acid (BMIPP). In Japan, Na^{123}I is only available in the form of a powder contained in a capsule, which is not usable for a phantom study. Therefore, we used ^{123}I-BMIPP, a liquid radiopharmaceutical, to mix homogeneously with agar. In the thyroid phantoms, 1.85 - 27.8 MBq of ^{99m}Tc pertechnetate or 0.37 - 3.7 MBq of ^{123}I-BMIPP were included. Plastic bottles were filled with 0.03 MBq/ml of ^{99m}Tc pertechnetate or 0.006 MBq/ml of ^{123}I BMIPP for background. These background tracer concentrations were determined using a previous thyroid phantom experiment as a reference (*24*). The neck phantom was placed in a supine position, and imaging was performed in the following order: 1. CZT-SPECT and 2. NaI camera, for 10 minutes each. After acquiring these images, the thyroid phantoms were divided into two pieces (right and left lobes); the radioactivity of each lobe was then measured using an automatic well counter and their volumes were measured using a measuring cylinder.

Parathyroid imaging

We simulated the following three different acquisition protocols: 1. dual-phase ^{99m}Tc-sestamibi protocol; 2. dual-isotope ^{99m}Tc sestamibi/^{99m}Tc pertechnetate protocol; and 3. dual-isotope ^{99m}Tc sestamibi/^{123}I iodine protocol.

The radiotracer dosage of each phantom in these three protocols is shown in Table 1. ^{99m}Tc-sestamibi was substituted with ^{99m}Tc pertechnetate in all our phantom studies since both tracers have the same photo energy of ^{99m}Tc. All the scanning procedures were performed using CZT-SPECT for 10 minutes.

(1) Dual-phase ^{99m}Tc sestamibi protocol

^{99m}Tc sestamibi accumulates in both parathyroid adenoma and thyroid tissue as a function of blood flow, gland size, and mitochondrial activity (*15,17*). However, ^{99m}Tc sestamibi washes out more rapidly from thyroid tissue than from parathyroid adenoma (*15,16*). Because of the difference in washout rate from the two tissues, a parathyroid adenoma is detected more clearly in a delayed phase image than in an early phase image. Thus, we prepared two type of neck phantoms to mimic the early phase and delayed phase neck images.

On the basis of preliminary experiments, including prior thyroid imaging, we determined the radioactivity of the early phase phantom. Subsequently, the radioactivity of the thyroid gland in the delayed phase phantom was determined, using a previous study for reference (*25*). In that study, the washout rate of ^{99m}Tc sestamibi from thyroid tissue was 0.013 at 180 minutes after administration. This value was approximately 13% of the radioactivity of the early phase image (at 20 minutes after administration). Generally, no biological washout of the ^{99m}Tc sestamibi was observed from the parathyroid adenoma; hence, we calculated the radioactivity of the parathyroid adenoma in the delayed phase only on the basis of physical decay of ^{99m}Tc, which was similar to the background. After calibration, these early and delayed neck phantoms were imaged.

(2) Dual-isotope ^{99m}Tc sestamibi/^{99m}Tc pertechnetate protocol

Although ^{99m}Tc sestamibi accumulates in both parathyroid adenomas and thyroid tissue, ^{99m}Tc pertechnetate accumulates only in thyroid tissue, not in a parathyroid adenoma. Thus, by subtracting a ^{99m}Tc pertechnetate image from a ^{99m}Tc sestamibi image, a parathyroid adenoma image could be obtained (*16,18*).

We constructed two types of neck phantoms. A single-tracer phantom to imitate a ^{99m}Tc pertechnetate image contained ^{99m}Tc pertechnetate in the thyroid gland, but not in the parathyroid adenoma. A dual-tracer phantom that simulated ^{99m}Tc sestamibi and ^{99m}Tc pertechnetate images contained ^{99m}Tc pertechnetate in both the thyroid gland and the parathyroid adenoma. We set reference markers on the neck phantom and scan bed to reproduce the position of phantoms consistently. First the single-tracer phantom was scanned. We then changed the single-tracer phantom to a dual-tracer phantom using the reference markers as a guide in order to maintain their scan positions. The dual-tracer phantom was then imaged.

(3) Dual-isotope ^{99m}Tc sestamibi/^{123}I-iodine protocol

Sodium ^{123}I-iodide accumulates only in the thyroid tissue, and ^{99m}Tc sestamibi accumulates in both a parathyroid adenoma and the thyroid tissue. By subtracting a ^{123}I-iodine image from a ^{99m}Tc sestamibi image, the uptake in the parathyroid adenoma is isolated (*16*).

We prepared the thyroid phantom to include both ^{99m}Tc pertechnetate and ^{123}I-BMIPP, while the parathyroid adenoma phantom only included ^{99m}Tc pertechnetate. The background included both ^{99m}Tc pertechnetate and ^{123}I-BMIPP. Dual-energy simultaneous acquisition of ^{99m}Tc and ^{123}I was performed. After acquisition, we generated ^{99m}Tc and ^{123}I window images separately, and subtracted the ^{123}I window image from the ^{99m}Tc window image.

Image acquisition and processing

In this study, we used D-SPECT (Spectrum Dynamics Medical, Israel) for CZT-SPECT imaging. D-SPECT is equipped with tungsten parallel-hole collimators and uses list-mode acquisition, with 120 projections per detector. The matrix size of CZT-SPECT images was 16 × 64 and the pixel size was 2.26 mm/pixel. CZT-SPECT data were reconstructed using the ordered subset expectation maximization method, with 7 iterations and 32 subsets. When we performed dual-isotope acquisition with the ^{99m}Tc and ^{123}I windows, two different energy windows were used simultaneously without scatter correction. The NaI camera (BrightView, Philips, Netherlands) was equipped with a low-energy, high-resolution collimator. The matrix size of the planar image from the NaI camera (NaI-planar image) was 256 × 256 and the pixel size was 6.4 mm/pixel. The details of the energy windows used for the CZT-SPECT and NaI cameras are shown in Table 2.

All images were analyzed using freely downloaded software for nuclear medicine (Prominence Processor Version 3.1, The Japanese Society of Radiological Technology, Tokyo, Japan) (*26*). Using this software, we made maximum intensity projection (MIP) images from the CZT-SPECT data. MIP images were generated by the same method used to make MIP images of NaI images (*27*). The maximum intensity along the viewing path was projected. We also used the "planar H/M" application program, which was installed on the D-SPECT workstation (*3*). This application was programmed to evaluate the heart-to-mediastinum ratio in cardiac ^{123}I-metaiodobenzylguanidine scintigraphy. Each detector of D-SPECT provides a small 2-D image per angular position. Taken together all the small 2-D images that share the same angle yield wide 2-D planar equivalent (PE) images, which look similar to planar images from a NaI camera.

In thyroid imaging, we set a region of interest (ROI) on both lobes of the thyroid gland and the background and measured the mean counts per pixel. Image counts for the ROI were calculated by subtracting the background mean counts from the ROI mean counts. In parathyroid imaging, image subtraction was performed using dual-isotope protocols on the MIP image. We adjusted the phantom position and uptake intensity between different photopeak images for subtraction using the software, and subjectively satisfactory images for diagnosis were thus obtained.

Statistical analysis

The data were analyzed using a website for statistical computation (VassarStats; http://vassarstats.net/). Correlations between the radioactivity and image counts were assessed using the Pearson's correlations coefficient (r). The differences in correlation coefficient between images were assessed using the Fisher transformation test. A two-tailed p value of <0.05 was considered statistically significant.

Results

Thyroid imaging

Typical images obtained using three different methods are shown in Figure 1. MIP images could depict the thyroid gland with good image quality; however, PE images were inferior to MIP and NaI-planar images in both the ^{99m}Tc and ^{123}I windows.

The relationship between radioactivity and image counts is shown in Figures 2 and 3. MIP images and PE images showed statistically significant correlations between the radioactivity and image counts for both ^{99m}Tc ($r = 0.93, 0.97, p < 0.05$) and ^{123}I images ($r = 0.89, 0.99, p < 0.05$). Similar results were obtained using the NaI-planar images for the ^{99m}Tc and ^{123}I windows ($r = 0.98, 0.99, p < 0.05$, respectively). The correlations between radioactivity and image counts of ^{99m}Tc radiotracer were not significantly different between MIP and PE images ($p = 0.54$). However, with the ^{123}I radiotracer, PE images had significantly stronger correlations than the MIP images ($p < 0.05$).

Parathyroid imaging

Figure 4 shows the dual-phase ^{99m}Tc sestamibi protocol. Early phase image depicted tracer uptake in the thyroid gland, with regional emphasis on the parathyroid adenoma in the lower quadrant of the left thyroid lobe. A clear accumulation in the parathyroid adenoma was visible in the simulated delayed phase image.

Figure 5 shows the dual-isotope ^{99m}Tc sestamibi/^{99m}Tc pertechnetate protocol. Dual-tracer images showed tracer uptake in the thyroid gland and parathyroid adenoma, while single-tracer images showed tracer uptake in the thyroid gland only. Subtraction of the single-tracer image from the dual-tracer image showed the parathyroid adenoma unmistakably.

Figure 6 shows the dual-isotope ^{99m}Tc sestamibi/^{123}I-iodine protocol. The ^{123}I photopeak image showed tracer uptake in the thyroid gland. In contrast, the ^{99m}Tc photopeak image showed tracer uptake in the thyroid gland and parathyroid adenoma; however, identifying the parathyroid adenoma was difficult. After subtraction of the ^{123}I photopeak image from the ^{99m}Tc photopeak image, the parathyroid adenoma was discernable.

Discussion

Thyroid imaging and quantitative analysis

Cardiac CZT-SPECT does not directly generate planar images, and most thyroid imaging is performed using a 2-D approach. Thus, we needed to convert tomographic data to 2-D data for a corresponding thyroid assessment. After a MIP image was generated, it could depict the thyroid gland as effectively as images from a NaI camera. In contrast, PE images were not adequate for visual assessment of the thyroid gland. The reason of this phenomenon is unclear, because this technique is theoretically similar to that performed with a NaI camera (*3*). At the least it can be concluded that an MIP image needs to be generated for visual assessment of the thyroid gland using cardiac CZT-SPECT.

Image counts measured by setting an ROI on the CZT-SPECT and NaI scans were significantly correlated in both the ^{99m}Tc and ^{123}I images. However, a detailed inspection revealed that in the MIP images, the regression line of the correlation did not cross the origin of the coordinates. Because an MIP image visualized plane the voxels with maximum intensity that fall in the way of parallel rays traced from the viewpoint to the plane of projection, the counts data might be overestimated. Thus, the approximate lines of the MIP image shifted to the higher count area. In addition, the PE images produced stronger correlations of radioactivity with image counts for the ^{123}I radiotracer than that for ^{99m}Tc. PE images were developed especially for calculation of the mean pixel counts of ^{123}I radiotracer (*3*). This property may be the reason for better quantification for the ^{123}I radiotracer compared with ^{99m}Tc.

Parathyroid imaging

In this study, we obtained clear parathyroid adenoma images in our phantom experiments which faithfully reproduce three different acquisition protocols using a CZT camera (*16*).

With the dual-phase ^{99m}Tc sestamibi protocol, a parathyroid adenoma can be visualized in a delayed phase image. Because dual-phase ^{99m}Tc sestamibi protocol is the most popular imaging protocol for parathyroid adenomas, our result indicates that this protocol may be one of the most feasible methods for the imaging of other organs using the CZT-SPECT instead of an NaI camera. To clarify this issue, further studies that include various sizes and radioactivities of a parathyroid adenoma are needed.

In the dual-isotope ^{99m}Tc sestamibi/^{99m}Tc pertechnetate protocol, we also obtained a good image of a parathyroid adenoma. Although several position gaps appeared between two different neck phantoms, software-based registration can permit high quality subtraction to clearly emphasize a parathyroid adenoma. Thus, this protocol also seems to be acceptable for parathyroid imaging by CZT-SPECT. In the clinical setting, these two images are obtained without changing a patient's neck position, unlike in our study; thus, a much clearer and motionless parathyroid image would be expected in human imaging.

Because both images were acquired simultaneously, in the dual-isotope ^{99m}Tc sestamibi/^{123}I-iodine protocol, a parathyroid adenoma was clearly visualized by subtracting the ^{123}I photopeak image from the ^{99m}Tc photopeak image. Although the emission energies of these radiotracers are close and crosstalk has an influence on image quality, currently this protocol is often performed in routine practice using a NaI camera. CZT-SPECT has better energy resolution compared to a NaI camera; thus, CZT-SPECT is theoretically more suitable for the dual-isotope protocol using ^{99m}Tc and ^{123}I. Tunninen et al. report that the ^{99m}Tc sestamibi/^{123}I-iodine dual-tracer protocol is superior to the ^{99m}Tc sestamibi single-tracer protocol (*14*). Taieb et al. also report a high sensitivity using ^{99m}Tc sestamibi/^{123}I-iodine subtraction scintigraphy (*28*). Therefore, the dual-isotope ^{99m}Tc sestamibi/^{123}I-iodine acquisition using CZT-SPECT seems to be the best protocol for nuclear medicine imaging of the parathyroid. Further clinical studies are needed to clarify the clinical impact of this technology.

Limitations

In this study, we used the same radiotracer dosage and acquisition time for CZT-SPECT and the NaI camera because this preliminary study needed to compare these two modalities under the same condition. Theoretically, a protocol with a lower dose or shorter acquisition time can be used with CZT-SPECT. Therefore, in future studies the radiotracer dose and acquisition time should be reduced in order to take advantage of CZT-SPECT. Since the dual-isotope protocol increases the radiation exposure, we should attempt to reduce this with CZT-SPECT technology.

It is well known that a certain proportion of patients with hyperparathyroidism have an ectopic parathyroid adenoma (*29*). If an ectopic parathyroid adenoma was in the mediastinum, CZT-SPECT with limited field of view does not cover both the neck and mediastinum using onetime scanning. Typically, CZT-SPECT is used for cardiac imaging; thus, it would be acceptable to perform additional mediastinal imaging as is done in a cardiac study. However, further research is required.

Conclusions

To our knowledge, this is the first study that attempted imaging of the neck region using cardiac CZT-SPECT. A combination of MIP and PE images appears to be useful for visual and quantitative assessment of thyroid disease. MIP images can be used for the detection of parathyroid adenomas using several different protocols, including the dual-isotope method.

Disclosure

We report no potential conflicts of interest that are relevant to this article.

Acknowledgements

We thank Mr. Shoji Nono at Department of Radiology, National Cerebral and Cardiovascular Center for his technical assistance.

References

1. Bocher M, Brevis IM, Tsukerman L, Shrem Y, Kovalski G, Volokh L. A fast cardiac gamma camera with dynamic SPECT capabilities: design, system validation and future potential. *Eur J Nucl Med Mol Imaging.* 2010;37:1887-1902.

2. Koulikov V, Lerman H, Kesler M, Spair EE. ^{99m}Tc-MDP bone scintigraphy of the hand: comparing the use of novel cadmium zinc telluride (CZT) and routine NaI(Tl) detectors. *Eur J Nucl Med Mol Imaging Research.* 2015;5:63.

3. Bellevre D, Manrique A, Lagallois D, et al. First determination of the heart-to-mediastinum ratio using cardiac dual isotope (^{123}I-MIBG/^{99m}Tc-tetrofosmin) CZT imaging in patients with heart failure: the ADRECARD study. *Eur J Nucl Med Mol Imaging.* 2015;42:1912-1919.

4. Takahashi Y, Miyagawa M, Nishiyama Y, Kawaguchi N, Ishimura H, Mochizuki T. Dual radioisotopes simultaneous SPECT of ^{99m}Tc-tetrofosmin and ^{123}I-BMIPP using a semiconductor detector. Asia Oceania *J Nucl Med Biol.* 2015;3:43-49.

5. Einstein AJ, Blankstein R, Andrews H, et al. Comparison of image quality, myocardial perfusion, and left ventricular function between standard imaging and single-injection ultra-low-dose imaging using a high-efficiency SPECT camera: The MILLISIEVELT

study. *J Nucl Med.* 2014;55:1430-1437.

6. Gambhir SS, Berman DS, Ziffer J, et al. A novel high-sensitivity rapid-acquisition single-photon cardiac imaging camera. *J Nucl Med.* 2009;50:635-643.

7. Dijk JD, Jager PL, Ottervanger JP, et al. Minimizing patient-specific tracer dose in myocardial perfusion imaging using CZT SPECT. *J Nucl Med Technol.* 2015;43:36-40.

8. Kobayashi M, Matsunari I, Nishi K, et al. Simultaneous acquisition of ^{99m}Tc- and ^{123}I-labeled radiotracers using a preclinical SPECT scanner with CZT detectors. *Ann Nucl Med.* 2016;30:263-271.

9. Ko T, Utanohara Y, Suzuki Y, et al. A preliminary feasibility study of simultaneous dual-isotope imaging with a solid-state dedicated cardiac camera for evaluating myocardial perfusion and fatty acid metabolism. *Heart Vessels.* 2016;31:38-45.

10. Tasi CJ, Cheng CY, Wang LY, et al. Tc-99m imaging in thyroidectomized differentiated thyroid cancer patients immediately before I-131 treatment. *Nucl Med Commun.* 2016:37;182-187.

11. Gerard SK, Cavalieri RR. ^{123}I diagnostic thyroid tumor whole-body scanning with imaging at 6, 24, and 48 hours. *Clin Nucl Med.* 2002;27:1-8.

12. Bravo PE, Goudarzi B, Rana U, et al. Clinical significance of discordant findings

between pre-therapy ^{123}I and post-therapy ^{131}I whole body scan in patients with thyroid cancer. *Int J Clin Exp Med.* 2013;6:320-333.

13. Ozdemir D, Cuhaci FN, Ozdemir E, et al. The role of postoperative ^{99m}Tc pertechnetate scintigraphy in estimation of remnant mass and prediction of successful ablation in patients with differentiated thyroid cancer. *Nucl Med Commun.* 2016;37:640-645.
14. Tunninen V, Varjo P, Schildt J, et al. Comparison of five parathyroid scintigraphic protocols. *Int J Mol Imaging.* 2013;2013:921260.
15. Mariani G, Gulec SA, Rubello D, et al. Preoperative localization and radioguided parathyroid surgery. *J Nucl Med.* 2003;44:1443-1458.
16. Greenspan BS, Dillehay G, Intenzo C, et al. SNM practice guideline for parathyroid scintigraphy 4.0. *J Nucl Med Tech.* 2012;40:111-118.
17. Elgazzar AH, Anim JT, Dannoon SF, Farghaly MM. Ultrastructure of hyperfunctioning parathyroid glands: does it explain various patterns of ^{99m}Tc-sestamibi uptake. *World J Nucl Med.* 2017;16:145-149.
18. Keane DF, Roberts G, Smith R, et al. Planar parathyroid localization scintigraphy: a comparison of subtraction and 1-, 2-, and 3-h washout protocols. *Nucl Med Commun.* 2013;34:582-589.

19. Chaudhary V, Bano S. Thyroid ultrasound. *Indian J Endocr Metab.* 2013;17:219-227.

20. Vurdem UE, Acer N, Ertekin T, Savranlar A, Topuz O, Keceli M. Comparison of three volumetric techniques for estimating thyroid gland volume. *Turk J Med Sci.* 2012;42:1299-1306.

21. Spencer RP, Waldman R. Size and positional relationships between thyroid lobes in the adult as determined by scintillation scanning. *J Nucl Med.* 1965;6:53-58.

22. Fang L, Tang B, Hou D, Meng M, Xiong M, Yang J. Relationship between parathyroid mass and parathyroid hormone level in hemodialysis patients with secondary hyperparathyroidism. *BMC Nephrology.* 2015;16:82.

23. Randhawa PS, Mace AD, Nouraei SA, Sterns MP. Primary hyperparathyroidism: do perioperative biochemical variables correlate with parathyroid adenoma weight or volume? *Clin Otolarygol.* 2007;32:179-184.

24. Fujii H, Iwasaki R, Ogawa K, et al. Evaluation of parathyroid imaging methods with Tc-99m-MIBI –The comparison of planar images obtained using a pinhole collimator and a parallel-hole collimator- (article in Japanese). *Kakuigaku.* 1999;36:425-433.

25. Santos AO, Wittmann DE, Nogueria RO, et al. ^{99m}Tc sestamibi thyroid uptake in euthyroid individuals and in patients with autoimmune thyroid disease. *Eur J Nucl Med*

Mol Imaging. 2005;32:702-707.

26. Maeda H, Yamaki N, Azuma M. Development of the software package of the nuclear medicine data processor for education and research (article in Japanese). *Nihon Hoshasen Gijutsu Gakkai Zasshi.* 2012;68:299-306.
27. Komori T, Narabayashi I, Doi K, Sueyoshi K, Tatsu Y, Utsunomiya K. A case of local recurrent pheochromocytoma: usefulness of I-123 MIBG early SPECT and maximum intensity projection images *Clin Nucl Med.* 2000;25:285-287.
28. Taieb D, Hindle E, Grassetto G, Colletti PM, Rubello D. Parathyroid scintigraphy when, how, and why? A concise systematic review. *Clin Nucl Med.* 2012;37:568-574.
29. Grozavu C, Pantile D. Primary hyperparathyroidism through an ectopic parathyroid adenoma. *Chirurgia.* 2016;111:156-160.

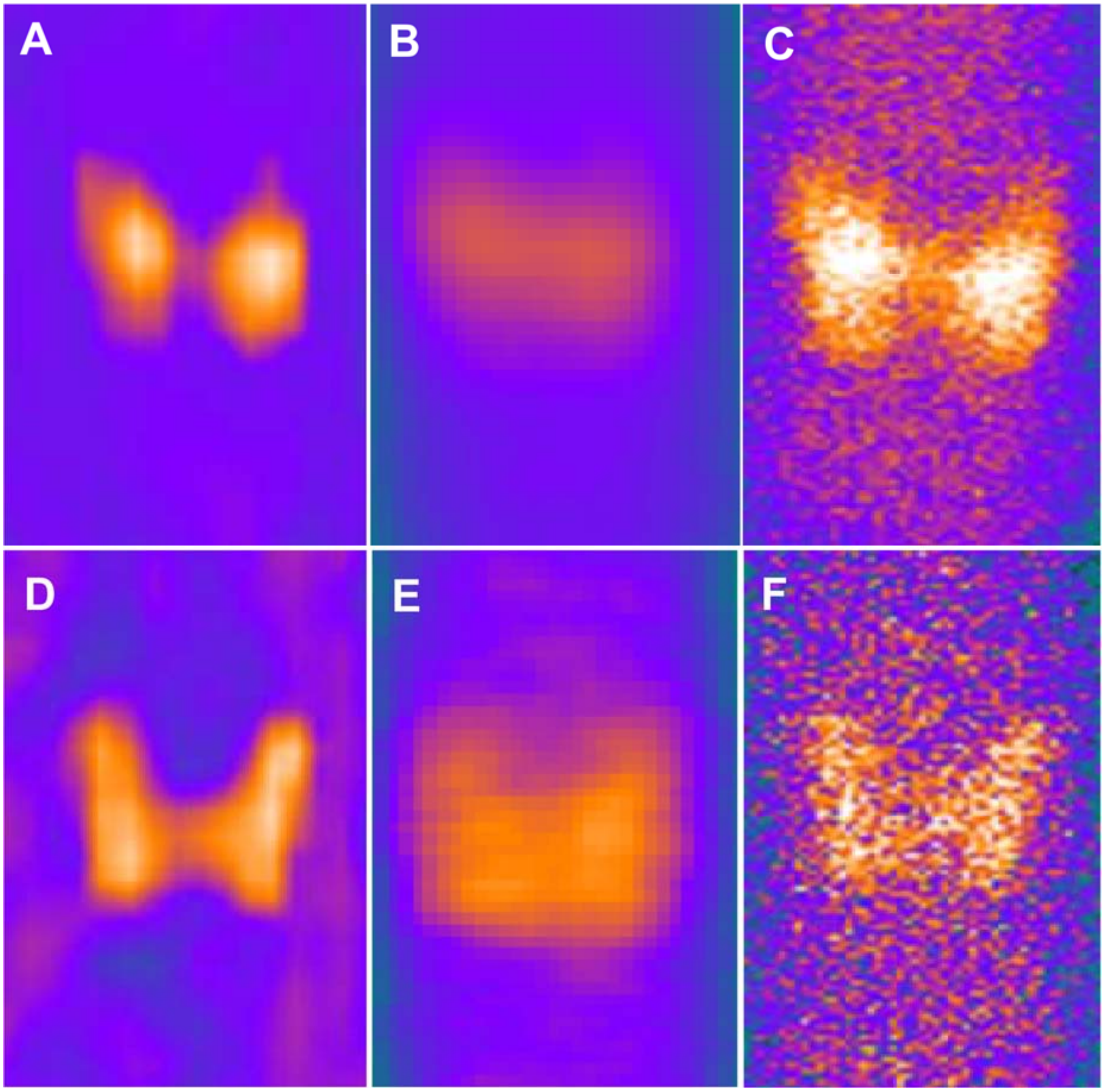

Figure 1.

Typical thyroid imaging using ^{99m}Tc (upper panel) and ^{123}I (lower panel) radiotracers.

(left column; MIP image, middle column; PE image, right column; NaI-planar image).

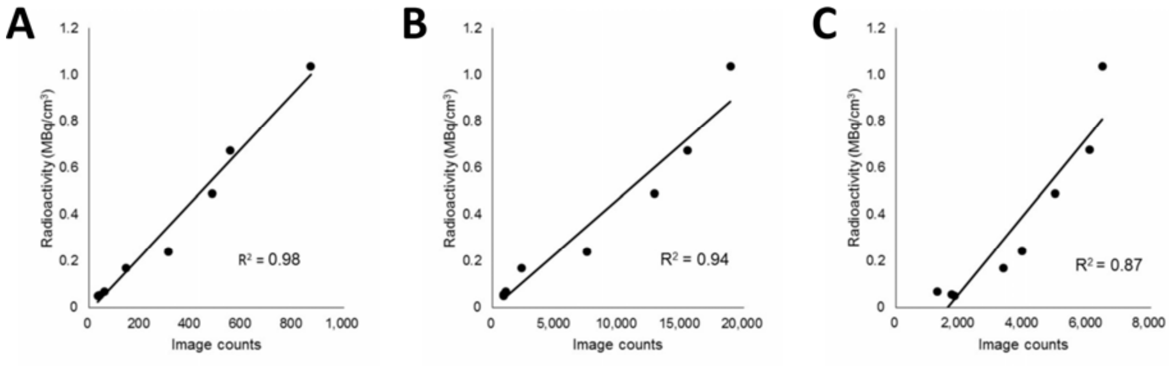

Figure 2.

The relationship between image counts and radioactivity of ^{99m}Tc-containing thyroid phantoms. A) NaI-planar image; B) MIP image; C) PE image.

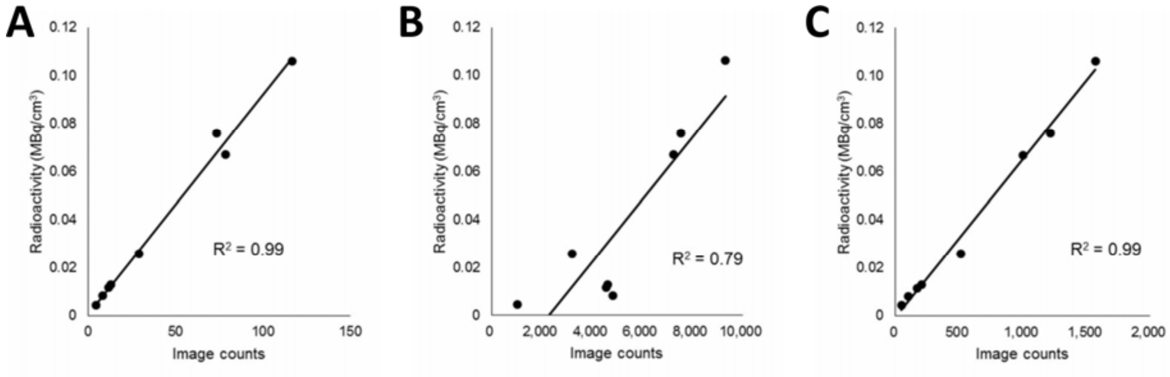

Figure 3.

The relationship between image counts and radioactivity of ^{123}I thyroid phantoms. A) NaI-planar image; B) MIP image; C) PE image.

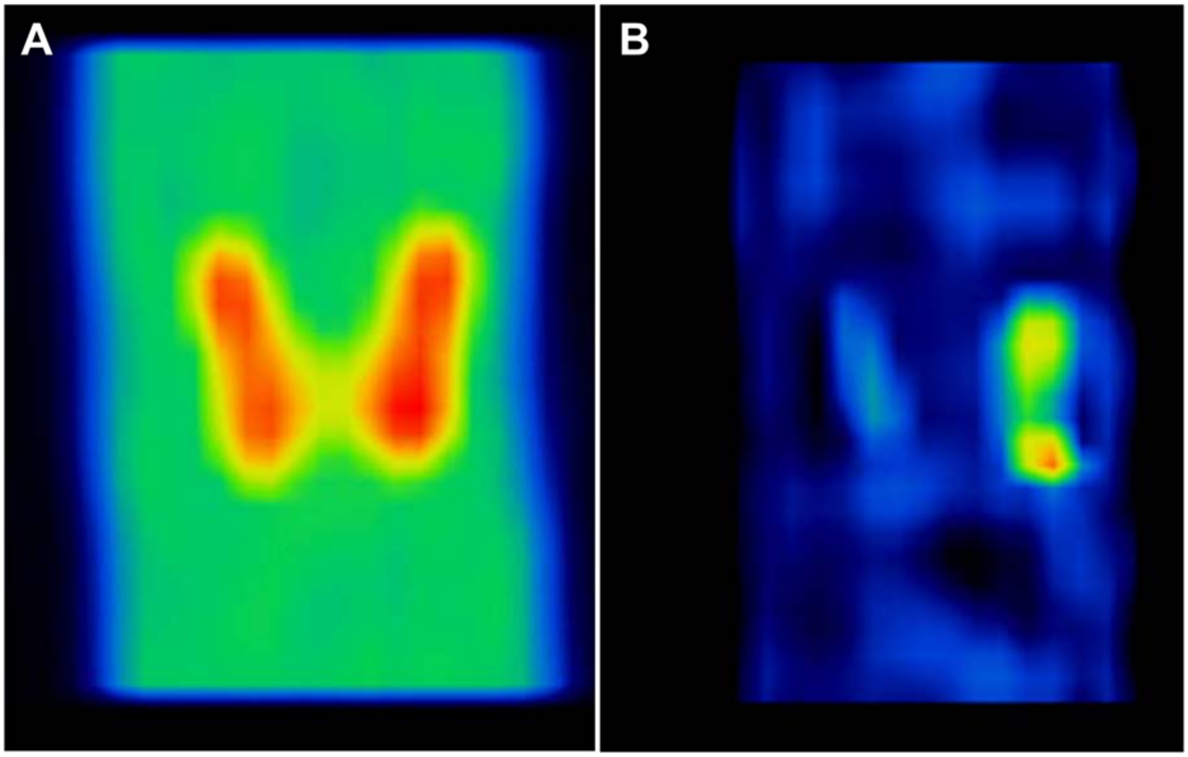

Figure 4.

Typical images from the dual-phase ^{99m}Tc sestamibi protocol using MIP images. A) Early phase image; B) delayed phase image. A clear accumulation of radiotracer is visible in the lower quadrant of the left thyroid lobe in the delayed phase image.

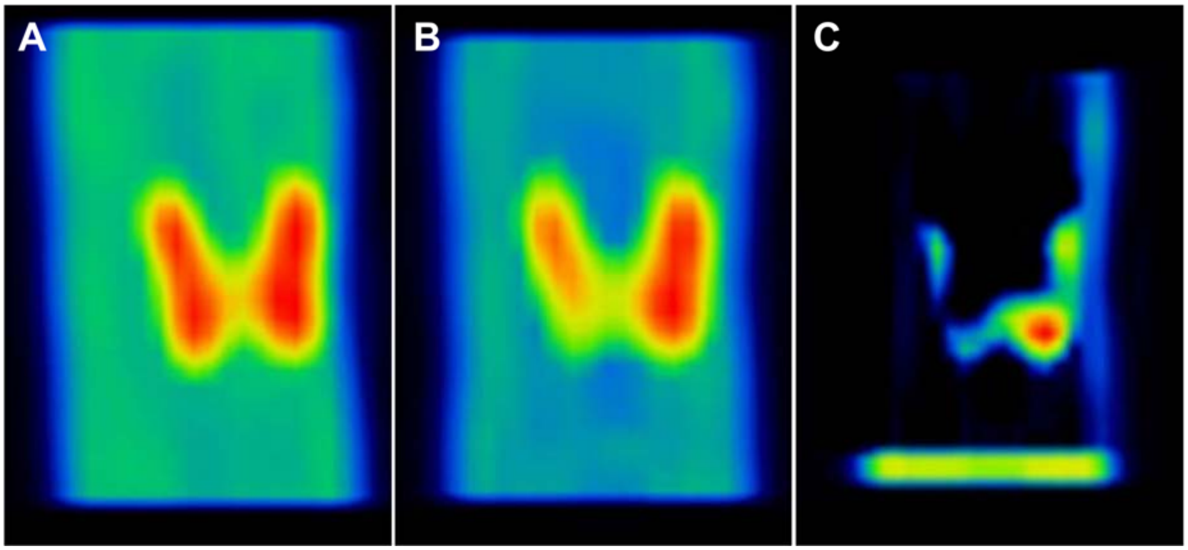

Figure 5.

Typical images from the dual-isotope ^{99m}Tc sestamibi/^{99m}Tc pertechnetate protocol using MIP images. A) Single-tracer image; B) dual-tracer image; C) subtracted image. After the single-tracer image was subtracted from the dual-tracer image, a solitary parathyroid adenoma was clearly visible.

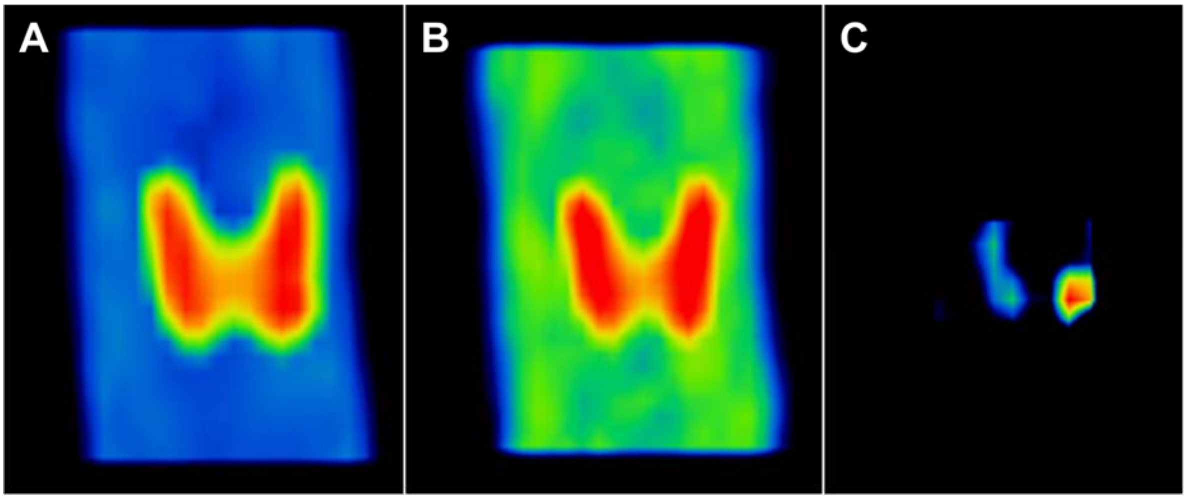

Figure 6.

Representative parathyroid images from the dual-isotope ^{99m}Tc sestamibi/^{123}I-iodine protocol using MIP images. A) ^{99m}Tc photopeak image; B) ^{123}I photopeak image; C) subtracted image. ^{99m}Tc-tracer is seen in the thyroid and parathyroid glands. A) ^{123}I is distributed in thyroid tissue. B) The parathyroid adenoma was then clearly visualized by subtracting the ^{123}I image from the ^{99m}Tc image.

Tables

TABLE 1

Radiotracer dosage of each phantom in the three parathyroid imaging protocols.

			Thyroid (MBq)	Parathyroid (MBq)	Background (MBq/ml)
Dual-phase ^{99m}Tc sestamibi	Early phase	^{99m}Tc	4.0	0.1	0.02
	Delayed phase	^{99m}Tc	0.5	0.07	0.014
Dual-isotope ^{99m}Tc sestamibi/^{99m}Tc pertechnetate	Single-tracer	^{99m}Tc	4.0	-	0.02
	Dual-tracer	^{99m}Tc	8.0	0.1	0.04
Dual-isotope ^{99m}Tc sestamibi/ ^{123}I iodine		^{99m}Tc	4.0	0.1	0.02
		^{123}I	0.74	-	0.006

TABLE 2

Energy windows used with CZT-SPECT and the NaI camera.

	Single-tracer acquisition		Dual-tracer acquisition
	CZT-SPECT (keV)	NaI camera (keV)	CZT-SPECT (keV)
^{99m}Tc window	140.5±10 %	140.5±15 %	140.5±5 %
^{123}I window	159±10 %	159±15 %	159±5 %